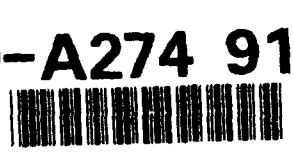

NAVAL POSTGRADUATE SCHOOL
MONTEREY, CALIFORNIA

THESIS

STUDY OF PRECIPITATION AND RECRYSTALLIZATION
IN Al ALLOY 2519 BY BACKSCATTERED
ELECTRON IMAGING METHODS

by

Peter Joseph Zohorsky

September 1993

Thesis Advisor: Terry R. McNelley

Unclassified

Security Classification of this page

REPORT DOCUMENTATION PAGE

1a Report Security Classification UNCLASSIFIED		1b Restrictive Markings	
2a Security Classification Authority		3 Distribution Availability of Report Approved for public distibution, distribution is unlimited	
2b Declassification Downgrading Schedule		5 Monitoring Organization Report Number(s)	
6a Name of Performing Organization Naval Postgraduate School	6b Office Symbol *(If Applicable)* *ME*	7a Name of Monitoring Organization Naval Postgraduate School	
6c Address *(city, state, and ZIP code)* Monterey, CA 93943-5000		7b Address *(city, state, and ZIP code)* Monterey,CA 93943-5000	
8a Name of Funding Sponsoring Organization	8b Office Symbol *(If Applicable)*	9 Procurement Instrument Identification Number	
8c Address *(city, state, and ZIP code)*		10 Source of Funding Numbers	
Program Element Number	Project No.	Task	Work Unit Accession No.

11 Title (Include Security Classification)
Study of Precipitation and Recrystallization in Al Alloy 2519 by Backscattered Electron Imaging Methods (unclassified)

12 Personal Author(s) Peter Joseph Zohorsky

13a Type of Report Master's Thesis	13b Time Covered From 01 93 To 09 93	14 Date of Report (year, month, day) September 1993	15 Page count 64

16 Supplementary Notation

17 Cosati Codes	Field	Group	Subgroup

18 Subject Terms *(continue on reverse if necessary and identity by block number)*
Aluminum-Copper alloys, grain refinement, particle stimulated nucleation (PSN), recrystallization

19 Abstract *(continue on reverse if necessary and identity by block number)*

This study examines the effects of pre-strain deformation temperature, overaging temperature, and other variations in thermomechanical processing (TMP) on the mean size and size distribution of q-phase precipitate particles in Al alloy 2519. Examination was performed using the scanning electron microscope in the backscattered imaging mode and quantitative image analysis methods were employed. The goal was to find a combination of TMP parameters which produces q-phase particles exceeding a critical diameter for particle stimulated nucleation (PSN) of recrystallization. A necessary prerequisite for superplasticity is a uniformly fine, equiaxed grain size and PSN is theorized to be capable of such grain refinement. Such a microstrucure has been developed in Aluminum alloys containing large second phase particles when the alloys are subjected to cold work and recrystallization treatments.

20 Distribution Availability of Abstract X unclassified unlimited same as report DTIC users	21 Abstract Security Classification UNCLASSIFIED	
22a Name of Responsible Individual Terry R. McNelley	22b Telephone *(Include Area Code)* (408) 656-2589	22c Office Symbol ME/Mc

DD FROM 1473, 84 MAR 83 APR edition may be used until exhausted security classification of this page
All other editions are obsolete Unclassified

Approved for public release; distribution is unlimited

STUDY OF PRECIPITATION AND RECRYSTALLIZATION IN Al ALLOY 2519 BY BACKSCATTERED ELECTRON IMAGING METHODS

by
Peter Joseph Zohorsky
Lieutenant, United States Coast Guard
B.S., United States Coast Guard Academy, 1983

Submitted in partial fulfillment
of the requirements for the degree of

MASTER OF SCIENCE IN MECHANICAL ENGINEERING

from the

NAVAL POSTGRADUATE SCHOOL
September 1993

Author: _____
Peter Joseph Zohorsky

Approved by: _____
Terry R. McNelley, Thesis Advisor

_____
Matthew D. Kelleher, Chairman
Department of Mechanical Engineering

ABSTRACT

This study examines the effects of pre-strain deformation temperature, overaging temperature, and other variations in thermomechanical processing (TMP) on the mean size and size distribution of θ-phase precipitate particles in Al alloy 2519. Examination was performed using the scanning electron microscope in the backscattered imaging mode and quantitative image analysis methods were employed. The goal was to find a combination of TMP parameters which produces θ-phase particles exceeding a critical diameter for particle stimulated nucleation (PSN) of recrystallization. A necessary prerequisite for superplasticity is a uniformly fine, equiaxed grain size and PSN is theorized to be capable of such grain refinement. Such a microstrucure has been developed in Aluminum alloys containing large second phase particles when the alloys are subjected to cold work and recrystallization treatments.

TABLE OF CONTENTS

I. INTRODUCTION

The phenomenon of superplasticity involves the elongation of certain metallic alloys to several hundred or even several thousand percent without failure due to localized necking. Some of the earliest research in this field was conducted in 1934 by Pearson who showed samples of Pb-Sn and Bi-Sn to exhibit elongations of up to 2000 percent [Ref.1]. Substantial amounts of Russian research in this field resulted in the universal term "superplasticity" being adopted from the translation of the Russian term for this phenomenon [Ref. 1]. There are two forms of superplasticity: transformation superplasticity and isothermal superplasticity. However, most research has concentrated on the latter form because of its ready applicability to industrial forming operations. Superplasticity allows the formation of complex and detailed parts from a single piece of metal through superplastic forming (SPF). Use of SPF reduces the weight of a structure and makes the structure easier to build and more reliable by reducing the number of parts, joints and fasteners. An example of the savings inherent in SPF is that of the girder assembly of the forward avionics lower deck of F-5E aircraft. Conventional construction would require 134 tools, 48 separate parts and nearly 45 manhours of labor. Introduction of SPF allows the use of only eight tools, five parts and less than 12 manhours [Ref. 2].

Research conducted at the Naval Postgraduate School involving Al alloy 2519 has been directed at the development of a TMP to produce superplasticity in this alloy. Mathe examined variations in the overaging time (from 12 minutes to 500 hours) and temperature (from 200°C to 500°C) by means of hardness testing and tensile testing. He also utilized optical microscopy and scanning electron microscopy to assess the size of the resulting θ-phase precipitates. He achieved 205 percent elongation from a sample overaged for ten hours at 450°C and then rolled at 350°C [Ref. 3]. Bohman used a single TMP overaging temperature of 450°C and times of either 10 or 50 hours [Ref. 4]. Extensive tensile testing was performed at temperatures between 300 and 450°C. Optical and scanning electron microscopy was employed to examine the microstructure at various points in the process and samples were also examined after tensile testing. An elongation of 260 percent was achieved at a testing temperature of 450°C following use of an overaging temperature of 450°C for 50 hours [Ref. 4]. In these studies [Refs. 3 & 4] the goal was to produce θ-phase precipitate particles large enough to serve as sites for particle stimulated nucleation (PSN) of recrystallization. Dunlap studied four different TMPs and performed scanning electron microscopy on the recrystallized samples. His TMP schedule was devised to attempt to improve on Bohman's work and involved variations in both the overaging and warm rolling steps. For PSN, the particles must exceed a critical size [Ref. 5] and Dunlap surmised that too few θ-phase particles greater the d_{crit} were

obtained. An analysis method was developed to estimate d_{crit} for each TMP and recrystallized grains of approximately 10-12 μm were achieved [Ref. 6].

The aim of our research at the Naval Postgraduate School is to find a TMP that results in optimal superplastic response for Al alloy 2519. This TMP may allow a relatively low forming temperature (such as that found previously for Al-Mg alloys of 300°C). Before this is possible, it is necessary to establish control of the precipitate size and distribution throughout the microstructure by varying the TMP [Ref. 7].

II. BACKGROUND

A. ALUMINUM AND ALUMINUM ALLOYS

Aluminum (Al) offers many desirable properties which make it such a widely used material. These properties include low density, high potential strength to weight ratio, high thermal and electrical conductivities, corrosion resistance and high ductility. Its high strength to weight ratio represents fuel savings and increased payload in military and transport applications [Ref. 8]. Alloying with a wide variety of elements enables the use of Aluminum products in military, automotive, aircraft, structural and general commercial applications.

The alloy studied in this research, Al alloy 2519, is a wrought Aluminum, 6 weight percent Copper (Cu) alloy of moderate strength with good weldability, corrosion resistance and cryogenic properties [Ref. 9]. The binary Aluminum-Copper phase diagram, shown in Figure 2.1, can be used directly to explain phase transformation processes [Ref. 10].

B. PHYSICAL METALLURGY OF AL ALLOY 2519

Precipitation hardening is the strengthening mechanism directly applicable to Al alloy 2519. The alloy derives most of its strength from Copper containing precipitate phases. Additional strength may be developed through strain hardening. In this research, it was intended to produce larger θ-phase particles than normally obtained

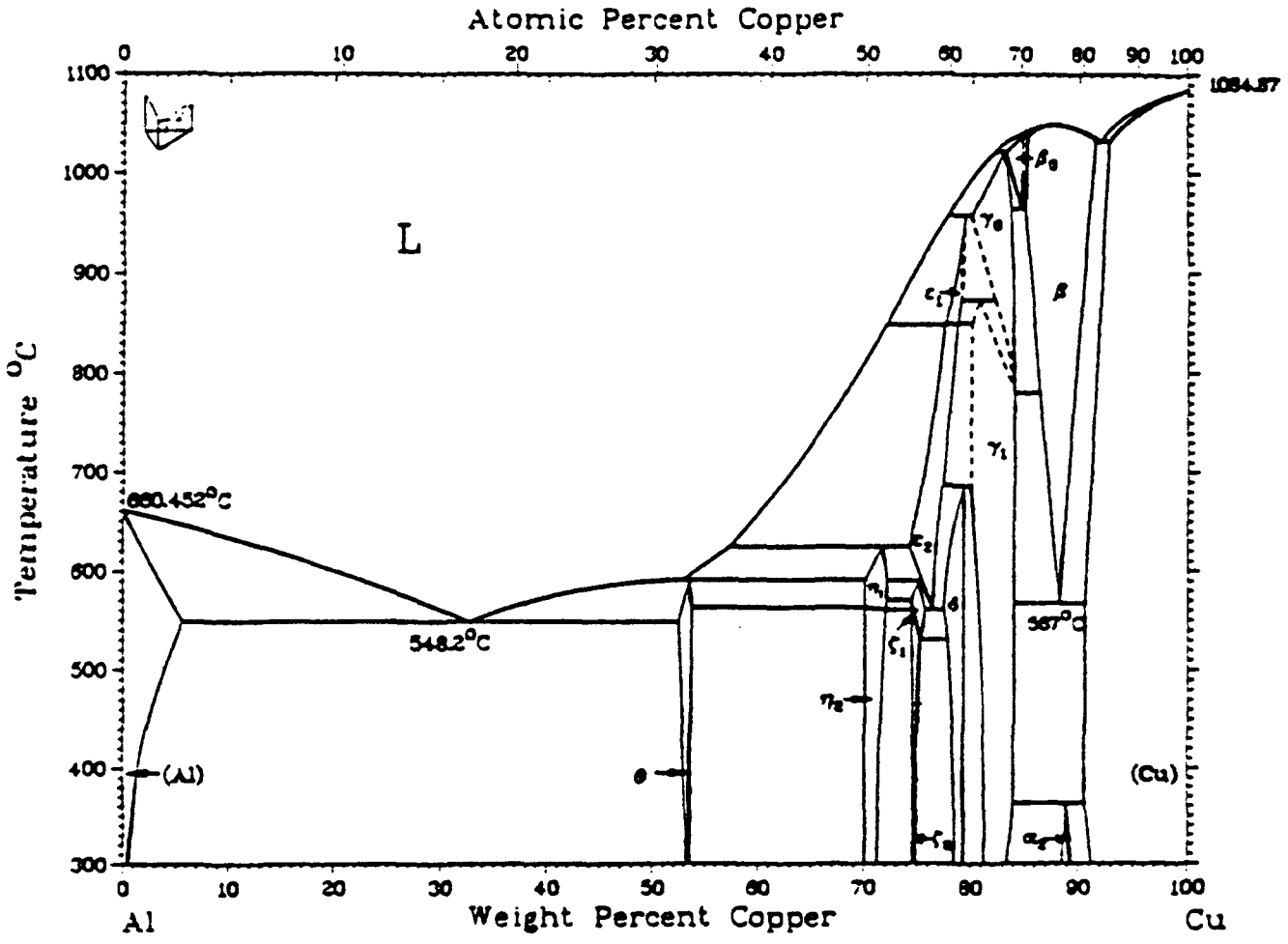

Figure 2.1 Al-Cu Phase Diagram [Ref. 10].

through precipitation hardening. The following sequence applies to the precipitation hardening of Al alloy 2519:

Supersaturated $\alpha \rightarrow$ GP zones $\rightarrow \theta'' \rightarrow \theta' \rightarrow \theta$

The metastable precipitates, which are Copper-rich, begin as a small clusters of atoms which change to discs or platelets and eventually transform to the equilibrium θ (Al_2Cu) phase [Ref. 11]. Control of the precipitation sequence involves assuring time and temperature conditions are met. Figure 2.2 shows the metastable solvus lines for Aluminum-Copper alloys as well as a time-temperature-transformation (TTT) curve for a hypothetical alloy of a content (denoted by "X") just below the maximum solubility of Copper in Aluminum (5.65 weight percent) [Ref. 12]. If an alloy containing θ' or θ'' precipitates is rapidly heated above their respective solvus these precipitates will dissolve, i.e., reversion takes place. Partial reversion can also occur below the solvus since the critical particle size decreases as temperature increases. A two-step overaging sequence following initial cold working was used to avoid such reversion and to aid in achieving a uniform distribution of θ-phase precipitates. The approximate solvus temperatures for the stable and metastable phases in Al alloy 2519 are: θ, 548°C; θ', 510°C; θ'', 280°C; and GP zones, 225°C [Refs. 13-15].

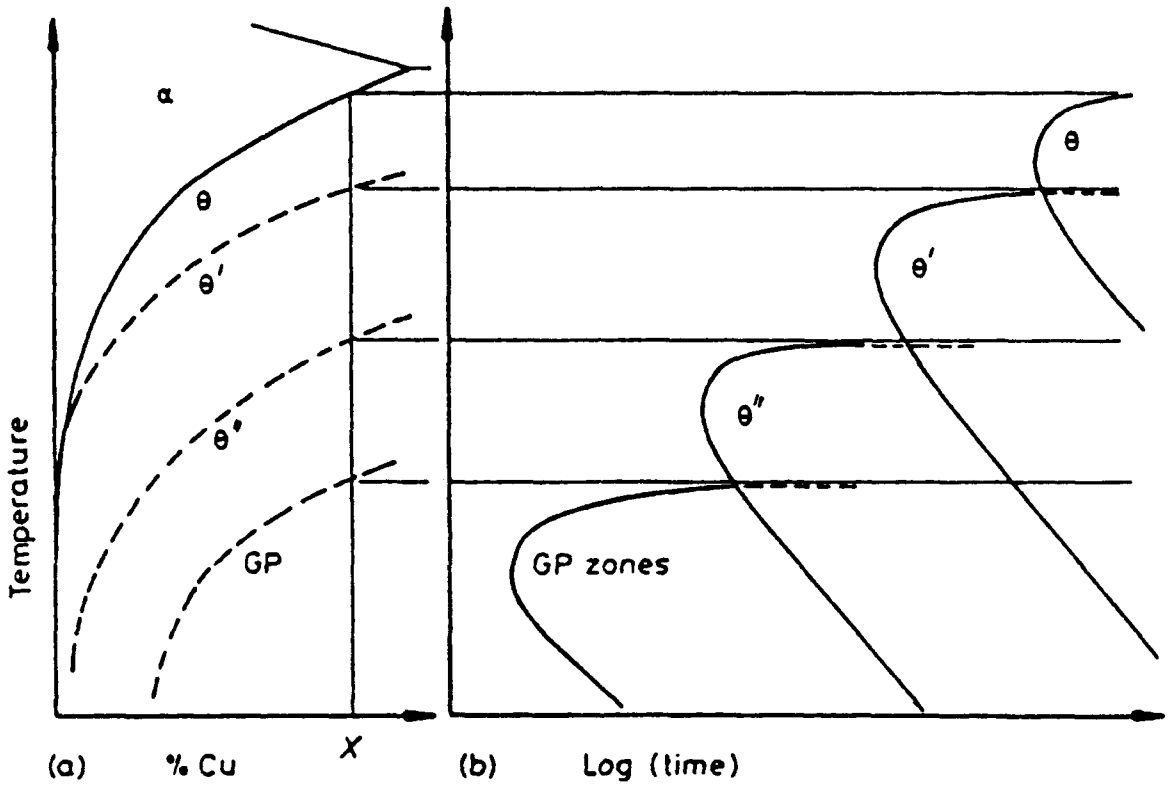

Figure 2.2 a) Al-Cu metastable phase solvus lines; b) TTT curve illustrating starting time for precipitation of various phases with X % Cu [Ref. 12].

C. GRAIN SIZE, RECRYSTALLIZATION AND SUPERPLASTICITY

A refined, equiaxed grain size is essential for superplasticity. Aluminum alloys undergo grain refinement by recrystallization through processes which include deformation and annealing.

Grain refinement by recrystallization in Al alloys requires the presence of particles to produce a fine grain size and can occur in the continuous (dynamic) mode (CRX) or the discontinuous (static) mode (DRX). Particles much less than 1.0μm in diameter (on the order of 10 -100 nm) may suppress nucleation and retard growth of recrystallized grains by retarding boundary migration, while particles greater than 1.0μm in diameter may become nucleation sites for recrystallized grains. The Supral process reportedly uses the CRX mode to obtain the prerequisite refined grain structure necessary for superplasticity. This process requires the addition of Zirconium (Zr), which forms fine precipitates of $ZrAl_3$ and which thus retards subgrain coarsening. Recrystallization to a fine grain size occurs as high-angle grain boundaries form during plastic deformation at an approximate temperature of 450°C [Ref. 16]. It has been suggested that new recrystallized grains do not nucleate in CRX. The success of this procedure has been attributed to the $ZrAl_3$ precipitates which control boundary migration and prevent DRX. Grain sizes using the Supral process are approximately 6μm [Ref. 17]. The introduction of 0.5 weight percent Zr to achieve this effect requires specialized melting and processing facilities.

The DRX mode requires a high density of nucleation sites for recrystallized grains [Ref. 16]. The Rockwell process utilizes DRX with Al-Zn-Mg-Cu alloys to obtain a refined grain size which is capable of producing a superplastic response. The method involves solution treatment, overaging, deformation and recrystallization. The critical steps in this procedure are the overaging and deformation stages. A single overaging treatment has been employed in association with severe deformation and annealing to induce recrystallization. Of note are the high recrystallization temperature (520°C) and high tensile test temperatures (also 520°C) [Ref. 18]. Precipitate particles between 0.5μm and 1.0μm in size produce a grain approximately 10μm in size using this process.

D. PSN THEORY

PSN of recrystallization may occur if favorable conditions regarding the size and distribution of θ-phase particles exist during deformation. These conditions are associated with the motion of dislocations in a deformation zone surrounding such particles during plastic deformation. Local lattice rotations associated with geometrically necessary dislocations may result from the presence of non-deforming particles [Ref. 5]. These dislocations are present in a density, ρ_g, given approximately by [Ref. 19]:

$$\rho_g = \frac{8f\varepsilon}{hd_p} \qquad (1)$$

where f is the volume fraction of particles, ε is the shear strain,

b is the Burgers vector and d_p is the particle diameter. The particle size and strain have a direct influence on the dislocation structure, as follows [Ref. 5]:

1. Small particles, i.e., $d_p < 0.1\mu m$, and low strains result in the dislocations forming prismatic loops which do not provide lattice rotations and consequently will not result in PSN;
2. Large particles, i.e., $d_p > 0.1\mu m$, and larger strains result in dislocation structures that do provide lattice rotations near the particles and so PSN may occur.

Continuum models use the strain hardening characteristics of the matrix to provide deformation zone size estimates as given by [Ref. 19]:

$$\lambda = A d_p \varepsilon^{\frac{n}{1-n}} \qquad (2)$$

where λ is the width of the deformation zone, A is a material constant, ε is the true axial strain and n is the strain hardening coefficient from Holloman's equation $\sigma = k\ \varepsilon^{n}$, where σ is true axial stress. Recrystallization embryos develop in association with lattice rotations within deformation zones of particles. These embryos, of size δ, must be smaller than the size of the deformation zone. In order for these embryos to be capable of growth [Refs. 5 & 20]:

$$\delta = \frac{4\Gamma}{E} \qquad (3)$$

Here, Γ is the grain boundary interfacial energy and E is the stored strain energy due to deformation. The associated free energy of formation, ΔG^*, of an embryo would be given by:

$$\Delta G^* = \frac{16\pi\Gamma^3}{3E^2} \qquad (4)$$

If PSN is to occur due to the stored strain energy within the deformation zone then δ must be less than or equal to λ [Ref. 21]. The conditions necessary for PSN are plotted schematically in Figure 2.3 and show this inverse nature of true strain versus particle diameter. This figure shows that PSN is easier to obtain for a particle with a larger diameter [Ref. 21].

An estimate of the grain size may be made assuming that all nucleated grains grow until they are prevented from further growth by each other. This becomes the particle spacing, D_S, and is given by [Ref. 22]:

$$D_s \approx \frac{d_p}{f^{\frac{1}{3}}} \qquad (5)$$

assuming all particles are larger than δ and become nucleation sites.

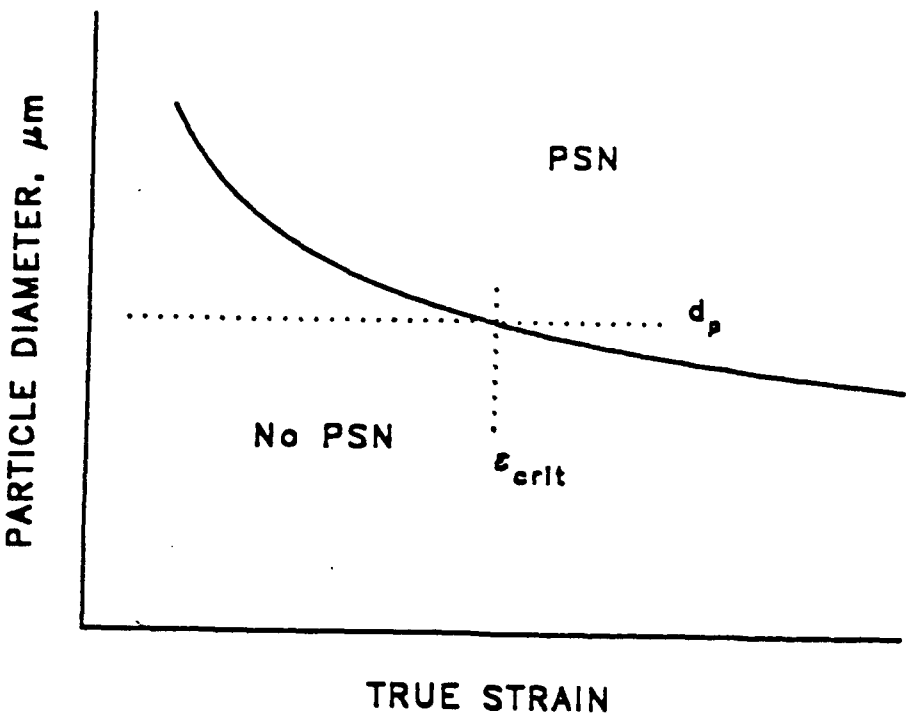

Figure 2.3 PSN model representing relationship between particle diameter and strain [Ref. 21].

E. CHANNELING CONTRAST

The resolution obtained by using the SEM is approximately 200 times greater than that of the optical microscope. In addition, if the SEM is operated in the backscatter detection (BSD) mode, atomic number differences and grain orientation differences are revealed [Ref. 14]. Using the SEM in the BSD mode enabled the θ precipitates to be easily identified. The θ precipitates (Al_2Cu) were brighter due to the higher average atomic number, compared to the surrounding Al matrix when the SEM was operated at 20 KV.

In order to examine the grain sizes and relative orientations, it was necessary to decrease the accelerating voltage to 6 KV, as reported by Dunlap [Ref. 6]. In this way, both the particles and the grains were evident.

III. EXPERIMENTAL PROCEDURE

A. MATERIAL

The material used in this research was supplied by the ALCOA Technical Center, ALCOA Center, Pennsylvania. The 2519 alloy was received as a rolled plate 0.875 in (22.2 mm) in thickness in the T87 temper condition. This means that the plate had been solution heat treated at 535°C, cold rolled seven percent and artificially aged for 24 hours at 165°C [Ref. 23].

The composition of the material, as analyzed by the manufacturer, is listed in Table 3.1.

TABLE 3.1: ALLOY COMPOSITION (WEIGHT PERCENT)

Cu	Mn	Mg	Fe	Zr	V	Si	Ti	Zn	Ni	Be	B	Al
6.06	0.30	0.21	0.16	0.13	0.04	0.07	0.06	0.03	0.01	0.002	0.001	bal

Sections were cut to 61.0 X 38.1 X 22.2 mm (2.4 X 1.5 X .875 in), with the longest dimension in the rolling direction of the plate.

B. PROCESSING

The thermomechanical processing of the material used in this research included five basic steps: 1) solution heat treatment; 2) low temperature prestrain; 3) overaging; 4) rolling (warm working); and 5) annealing (for recrystallization).

The samples were solution heat treated in a furnace for 100 minutes at 535°C. A room temperature water quench of the samples was then performed, resulting in a supersaturated solid solution. For the first series of samples, a ten percent prestrain at 200°C was then conducted, using the Fenn Laboratory rolling mill. This introduced dislocations to serve as nucleation sites for the θ' precipitates which precede the formation of θ-phase during low temperature aging. The ten percent reduction was achieved using two passes of five percent each. The second series of samples was rolled at 25°C and also achieved a ten percent reduction in two passes. Previous research here dealing with superplasticity of Al 2519 [Refs. 3, 4, 6] and of Al-Mg alloys suggested the elevated rolling temperature was required to avoid cracking during this 10 percent reduction. However, it was found that reductions of greater than 30 percent were possible at room temperature (25°C) with this alloy. Prestrain conducted at 25°C would result in a higher and more uniform dislocation density and thus a more uniform θ' distribution during subsequent aging [Ref. 7]. A more uniform distribution of θ would then be expected, resulting in a more highly refined grain size and better superplastic response [Ref. 22]. Also, the lower temperature prestraining is more applicable to industrial applications since it is more straight forward to perform.

The initial step in the overaging sequence that was performed on all samples was 50 hours in a oven set at 200°C. From this point, each sample underwent a separate heat treatment which lasted

either 50 or 100 hours at temperatures ranging from 350°C to 450°C. The processing is depicted schematically in Figure 3.1 (a) and (b). Figure 3.2 (a) and (b) represents the process in the form of a flowchart. In addition, one sample was overaged only for 50 hours at 200°C and another sample was overaged 200 hours at 200°C.

All samples were cooled in the furnaces until their temperatures reached 200°C. This was followed by a room temperature water quench. All samples were stored in a freezer maintained at -25°C while awaiting subsequent processing or examination.

C. SAMPLE PREPARATION

1. Grinding and Polishing

From the original sample, a smaller specimen was sectioned in order to prepare the transverse-longitudinal face for examination in the SEM. The surface to be examined, which had an area of approximately 1-2 cm^2, was ground unmounted using successively fine grits (220, 320, 500) of silicon carbide paper on the Struers Knuth-Rotor 3 grinder. Each specimen was polished using 6 μm and 1μm aerosol diamond compound. The 6 μm polish was performed using Buehler TEXMET polishing cloth at a speed of 400 rpm. The 1 μm polish was done using Buehler CHEMOMET polishing cloth at a speed of 200 rpm [Ref. 25]. A lubricant was also used with the 1 μm polish.

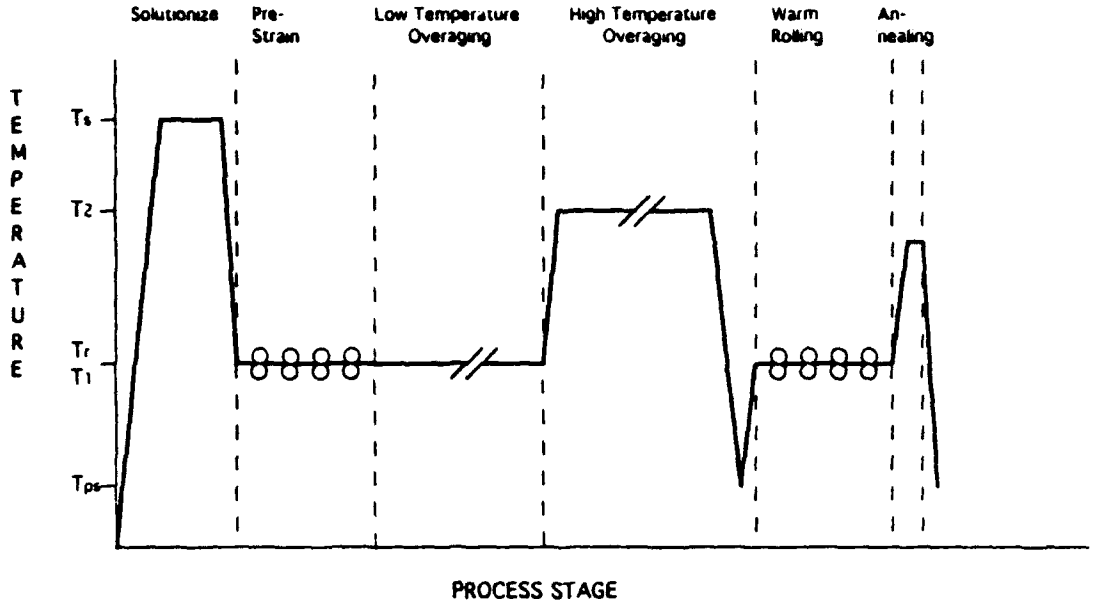

(a)

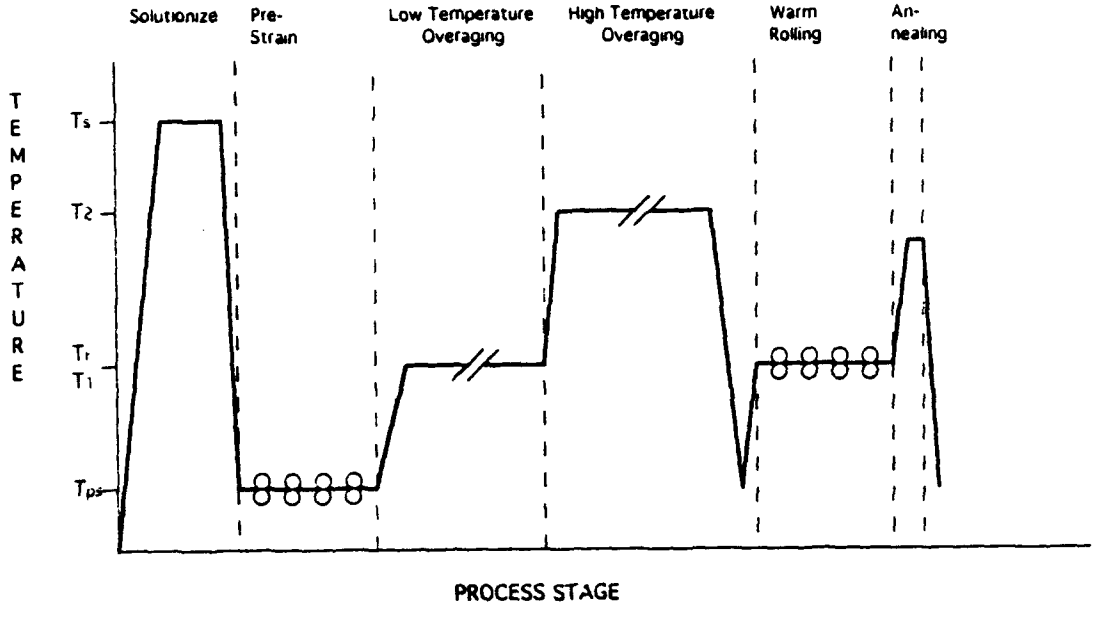

(b)

Figure 3.1 Processing schematic of the experiments conducted during a) series 1 and b) series 2.

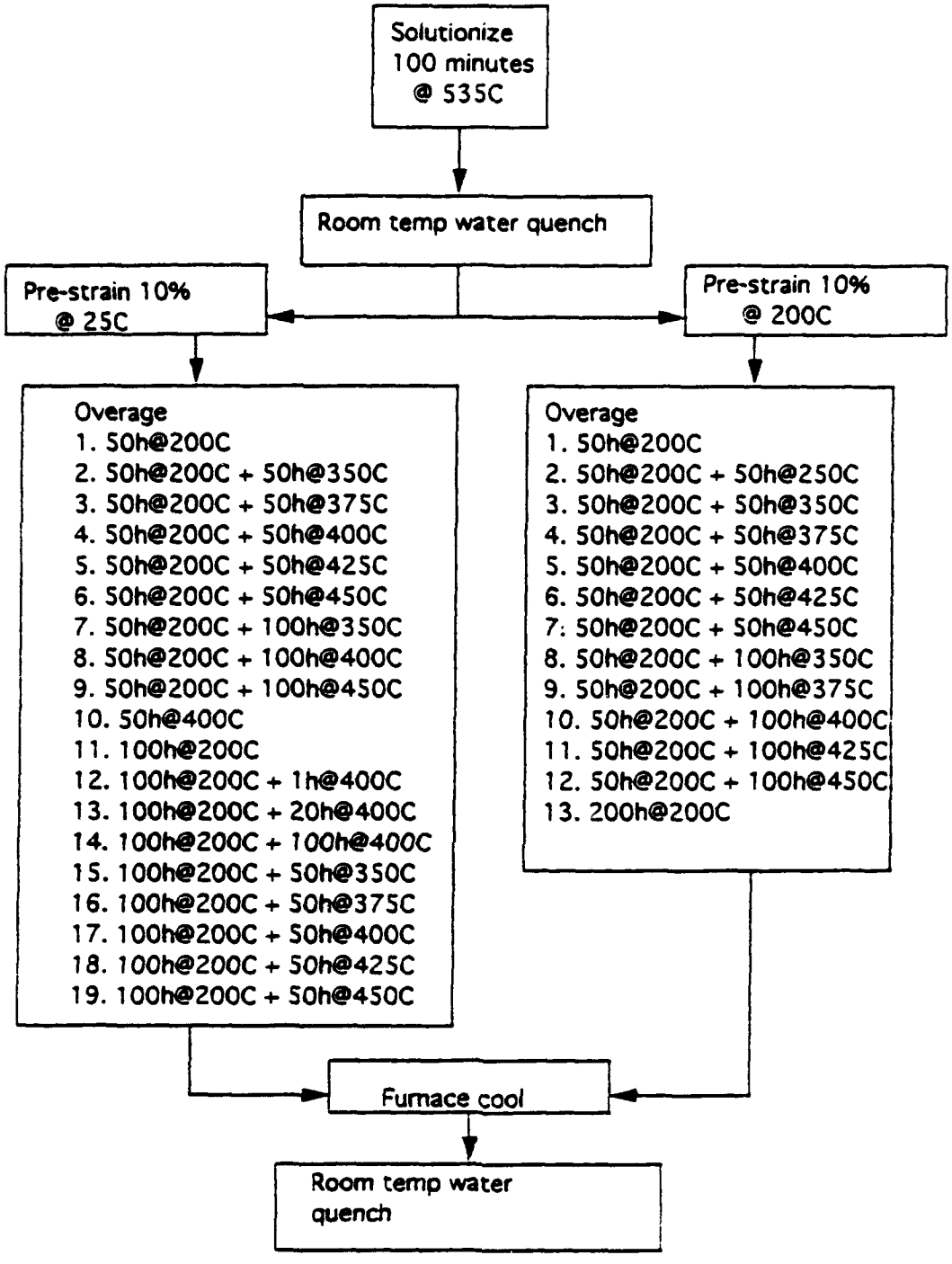

(a)

Figure 3.2 Process flowchart illustrating a) experimentation through overaging; (continued)

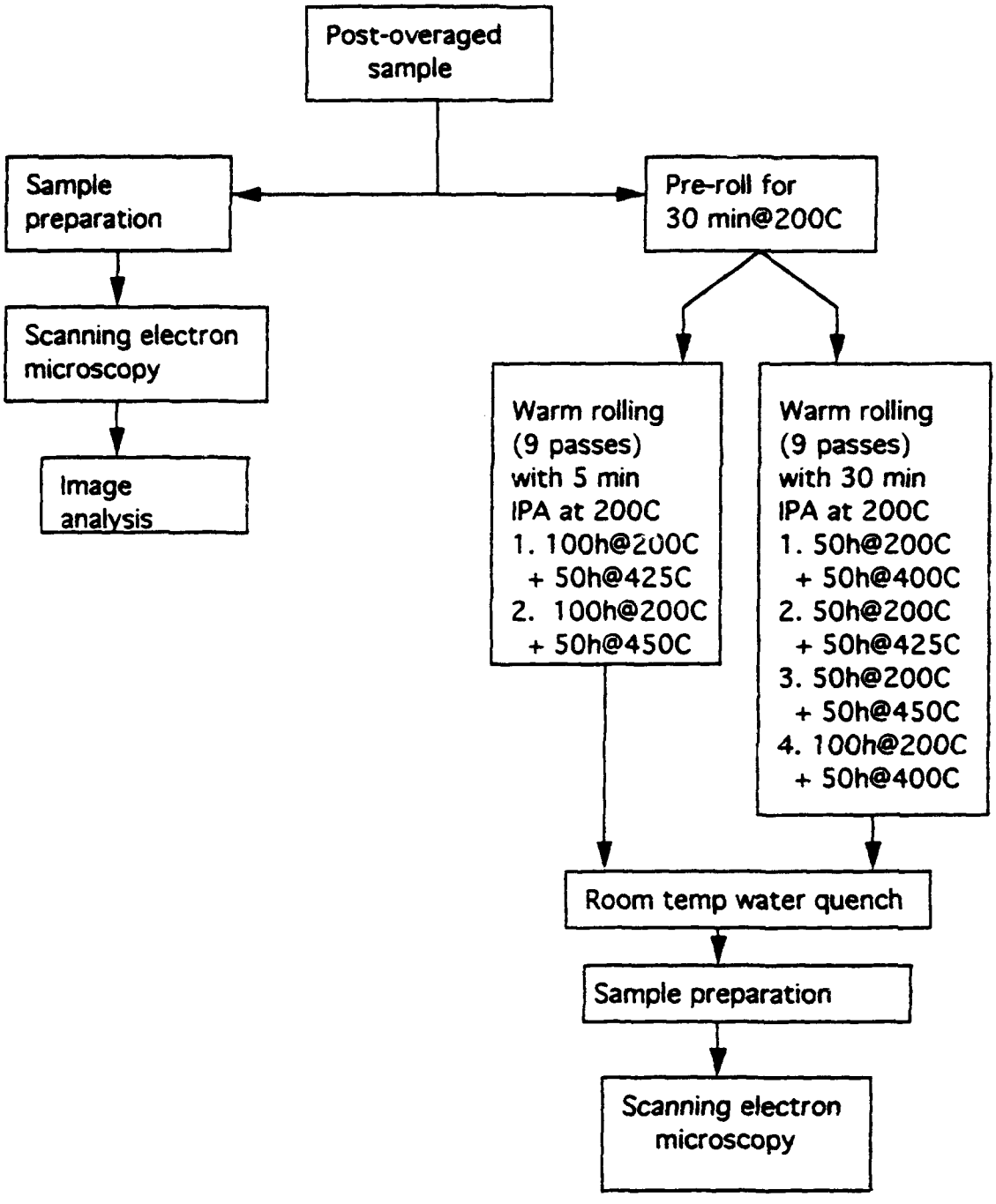

(b)

Figure 3.2 b) rolling, recrystallization and analysis.

Polishing continued until all scratches from the proceeding step were eliminated. At this time the specimen was rinsed with methanol and dried with a blower.

2. Electropolishing

Electropolishing was performed with a solution of 70 percent methanol and 30 percent nitric acid. This solution was contained in a stainless steel beaker. The beaker was surrounded by pure methanol in an insulated plastic container. During electropolishing both solutions were cooled to -20°C with liquid nitrogen and the sample was inserted into the electropolishing solution for two minutes at 7 VDC. The sample was then rinsed in a methanol bath.

3. Microscopy

All samples were examined with the SEM which was operated in the backscatter mode with an accelerating voltage of 20 KV using LaB_6 and tungsten filaments. When photographs were taken of the samples, the composition, magnification and contrast levels were chosen to provide similarity between photographs for an easier comparison between samples.

D. IMAGE ANALYSIS

Micrographs taken using the SEM were scanned into a personal computer and the data were analyzed using Image-Pro Plus 2.0 software. This analysis was performed in order to quantify the following parameters of the θ-phase particles: area, major axis length, aspect ratio, and average diameter. Data generated by this

image analysis was transferred into Excel 4.0 for data reduction and plotting of histograms. Histograms of the major axis and average diameter of the θ particles were plotted in order to assess the effect of process variation on the θ-phase particle size and size distribution.

E. WARM ROLLING

Table 3.2 summarizes the overaging conditions that were chosen for subsequent warm rolling as well as the associated interpass annealing (IPA) times. All samples chosen for warm rolling had received prestraining at 25° C.

TABLE 3.2: INTERPASS ANNEAL SCHEDULE

Overaging treatment	Interpass anneal time (minutes)
50h@200°C + 50h@400°C	30
50h@200°C + 50h@425°C	30
50h@200°C + 50h@450°C	30
100h@200°C + 50h@400°C	30
100h@200°C + 50h@425°C	5
100h@200°C + 50h@450°C	5

All of these samples underwent nine rolling passes which provided a total reduction of approximately 90 percent. After pass number nine, the samples were quenched in room temperature water and stored in the freezer for further recrystallization studies.

Using the rolling mill diameter as 4.0 inches with an angular velocity of 0.327 radians/second, the true strain, ε , and the strain rate, $\dot{\varepsilon}$, could be calculated for each pass using Equations 6 and 7 [Ref. 6].

$$\varepsilon = \ln\left(\frac{t_i}{t_f}\right) \tag{6}$$

$$\dot{\varepsilon} = \frac{2\pi R\omega}{\sqrt{Rt_i}}\sqrt{\varepsilon\left(1+\frac{\varepsilon}{4}\right)} \tag{7}$$

In these equations, t_i, is the initial sample thickness, t_f is the mill gap setting, R is the radius of the mill roller and ω is the angular velocity of the rolls. Table 3.3 summarizes the rolling process.

TABLE 3.3 ROLLING SCHEDULE

Roll pass #	Initial thickness (in)	Mill gap setting (in)	Final thickness (in)	Mill deflection (in)	True strain	Strain rate (s^{-1})
1	0.814	0.745	0.771	0.026	0.054	0.756
2	0.771	0.655	0.683	0.028	0.121	1.169
3	0.683	0.570	0.601	0.031	0.128	1.277
4	0.601	0.530	0.555	0.025	0.080	1.068
5	0.555	0.430	0.458	0.028	0.192	1.750
6	0.458	0.345	0.376	0.031	0.197	1.954
7	0.376	0.220	0.261	0.041	0.365	2.991
8	0.261	0.125	0.170	0.045	0.429	3.918
9	0.170	0.060	0.100	0.040	0.531	5.463

F. RECRYSTALLIZATION

From each of the pieces which had been warm rolled, a section was cut to a size of approximately 19.05 X 12.7 mm (0.75 X 1.5 in). These samples were then annealed at 375°C for ten minutes. Following this treatment the samples were quenched in water at room temperature and prepared for the SEM using the procedure previously mentioned. The samples were examined with the SEM in the backscatter mode with an accelerating voltage of 6 KV to examine the recrystallized grain structure and grain orientation.

The lower voltage results in improved contrast and better resolution of orientation contrast between grains.

G. X-RAY DIFFRACTION

X-ray diffraction analysis was conducted on the bulk (unpowdered) sample overaged for 50 hours at 200°C and 100 hours at 450°C to confirm the presence of θ-phase particles. This analysis was conducted using a Philips x-ray generator, diffraction controller, and automatic powder-diffraction software. The sample was scanned using CuKα radiation and identification of the phases present was accomplished using the previously mentioned software.

IV. RESULTS AND DISCUSSION

The various results obtained from this research will be discussed in an order consistent with the processing sequence given in Figure 3.1. An analysis of the SEM micrographs and histograms created using image analysis techniques and general observations will be employed in reporting the outcomes of the stages of this research.

A. MICROSCOPY

The SEM proved to be extremely effective by producing micrographs which revealed the similarities and differences between TMPs. Optical microscopy was attempted, late in the research, to reveal the grain contrast of anodized annealed samples using crossed polars. These efforts were unsuccessful. However, SEM micrographs were obtained of these annealed samples.

1. Series 1

Figure 3.1a represented materials that were prestrained at 200°C and then subjected to a two-step overaging treatment. Figure 4.1 shows the distribution of θ-phase particles in samples which were subjected to high temperature overaging for 50 hours at 350°C, 400°C and 450°C (a-c, respectively). The θ-phase forms on prior grain boundaries as well as within grain interiors. Higher overaging

(a)

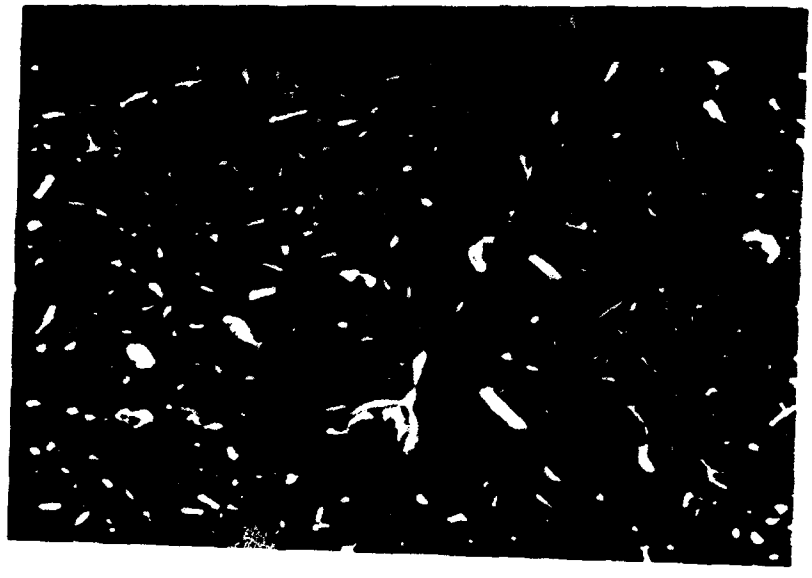

(b)

Figure 4.1 Backscattered electron micrographs showing grain boundaries of samples prestrained at 200°C and aged for 50 hours at 200°C and a) 50 hours at 350°C; b) 50 hours at 400°C; (continued)

(c)

Figure 4.1 c) 50 hours at 450°C.

temperature results in coarser θ-phase particles both on boundaries and in grain interiors. The coarser dispersion at higher overaging temperatures is consistent with conventional theories of nucleation and growth [Ref. 26].

Figure 4.2 shows micrographs including the grain boundary regions of samples that were subjected to a secondary aging for 100 hours at these same temperatures of 350°C, 400°C and 450°C. Ostwald ripening with the passage of time is evident upon comparison of Figures 4.1 and 4.2.

It also appears that the θ-phase particle size distribution is shifted to larger size as the overaging time increases. However, a precipitate-free zone (PFZ) is also evident and appears to be approximately the same when comparing samples with the same overaging temperature but different overaging time.

2. Series 2

Figure 3.1b illustrated the process for samples that were prestrained at 25°C and then underwent a two-step overaging. Micrographs shown in Figures 4.3 and 4.4 again demonstrate the effect of overaging time and temperature.

A direct comparison of micrographs representing material experiencing the same heat treatment and only differing with respect to prestrain temperature is possible in Figures 4.1 and 4.3. This comparison reveals the 25°C prestrain to result in smaller, more spherical particles within grain interiors and a better particle

(a)

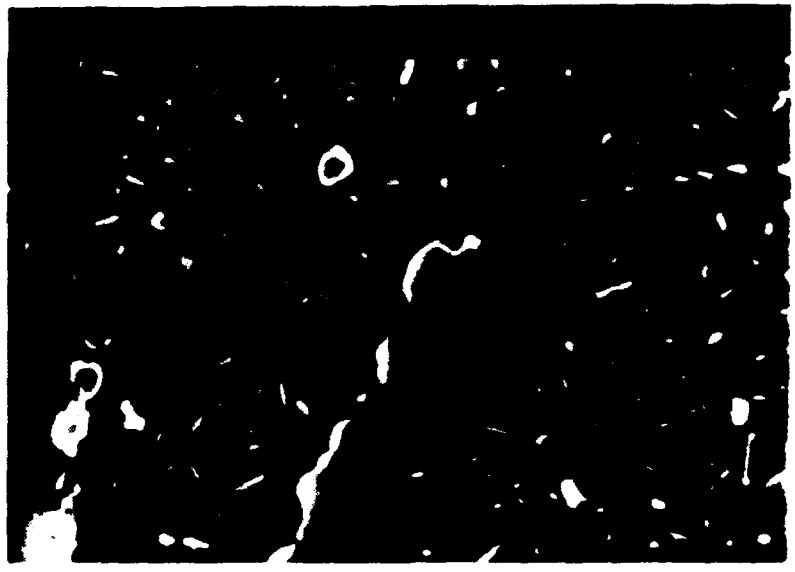

(b)

Figure 4.2 Backscattered electron micrographs showing grain boundaries of samples prestrained at 200°C and aged for 50 hours at 200°C and a) 50 hours at 350°C; b) 50 hours at 400°C; (continued)

(c)

Figure 4.2 c) 50 hours at 450°C.

(a)

(b)

Figure 4.3 Backscattered electron micrographs showing grain boundaries of samples prestrained at 25°C and aged for 50 hours at 200°C and a) 50 hours at 400°C; b) 50 hours at 450°C.

(a)

(b)

Figure 4.4 Backscattered electron micrographs showing grain boundaries of samples prestrained at 25°C and aged for 50 hours at 200°C and a) 100 hours at 400°C; b) 100 hours at 450°C.

size distribution, that is, a more uniform θ-phase particle size, was obtained following the 25°C prestrain. Figure 4.3a shows a microstructure that appears to possess a large number of equiaxed particles that are approximately 1 μm in average diameter.

Figure 4.5 shows micrographs of the matrix of samples that were prestrained at 25°C and were subjected to initial overaging at 200°C for times from one to 100 hours. The secondary overaging in these cases was accomplished at 400°C for 50 hours. In this way, the effectiveness of the initial 200°C overaging may be examined. The micrographs exhibit only minor changes with regard to θ-phase particle size and θ-phase particle size distribution, which implies that the initial overaging at 200°C is not a major factor in the overall microstructure of a sample that undergoes a two-step overaging sequence.

The effect of time at a secondary overaging temperature of 400°C is demonstrated in Figure 4.6. These samples, prestrained at 25°C with the initial overaging of 200°C for 100 hours, show that the particles are fewer in number and coarser as the high temperature overaging time increases. The number of particles increases dramatically between zero and one hour which again shows the importance of the high temperature overaging.

Finally, seven samples within series 2 were warm rolled to approximately 90 percent reduction, recrystallized and prepared for

(a)

(b)

Figure 4.5 Backscattered electron micrographs showing grain interiors (matrix) of samples prestrained at 25°C and with a secondary overaging of 400°C for 50 hours. Initial overaging was at 200°C for a) 0 hours; b) 50 hours; (continued)

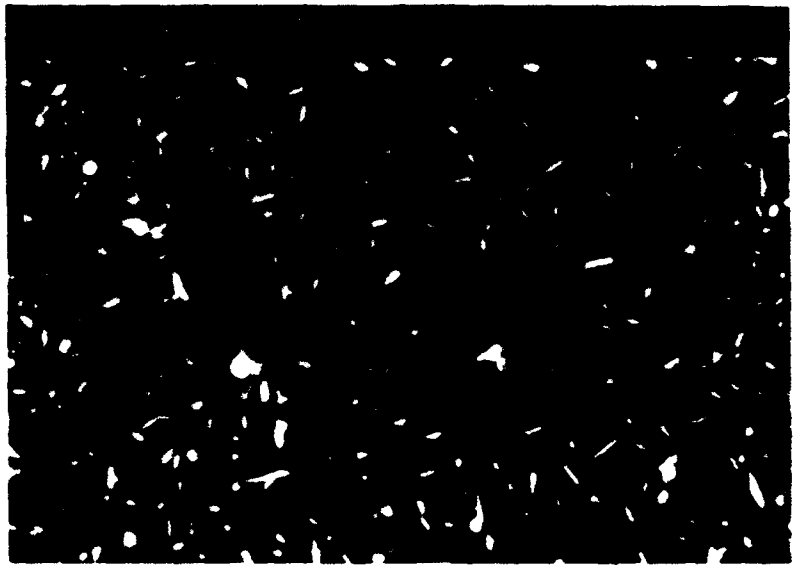

(c)

Figure 4.5 c) 100 hours at 200°C

(a)

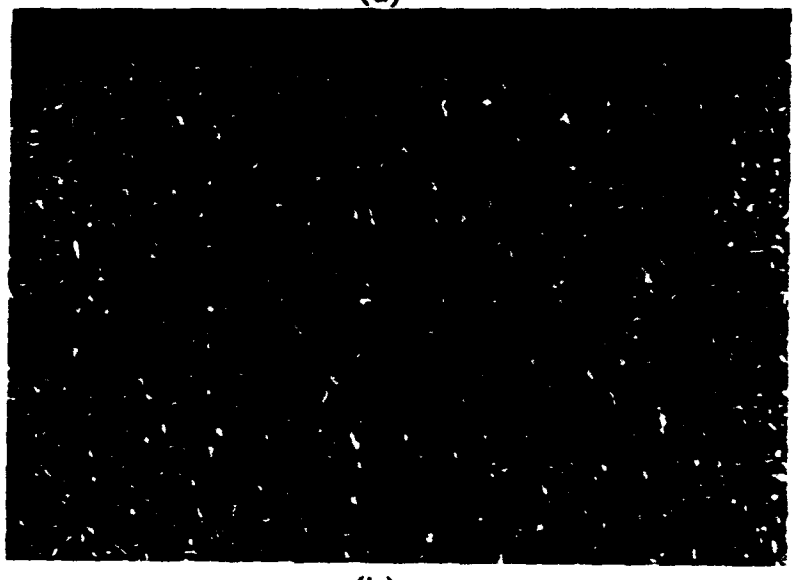

(b)

Figure 4.6 Backscattered electron micrographs showing grain interiors (matrix) of samples prestrained at 25°C and aged for 100 hours at 200°C. Secondary overage was conducted at 400°C for a) 0 hours; b) 1 hour; (continued)

(c)

(d)

Figure 4.6 c) 20 hours; d) 50 hours; (continued)

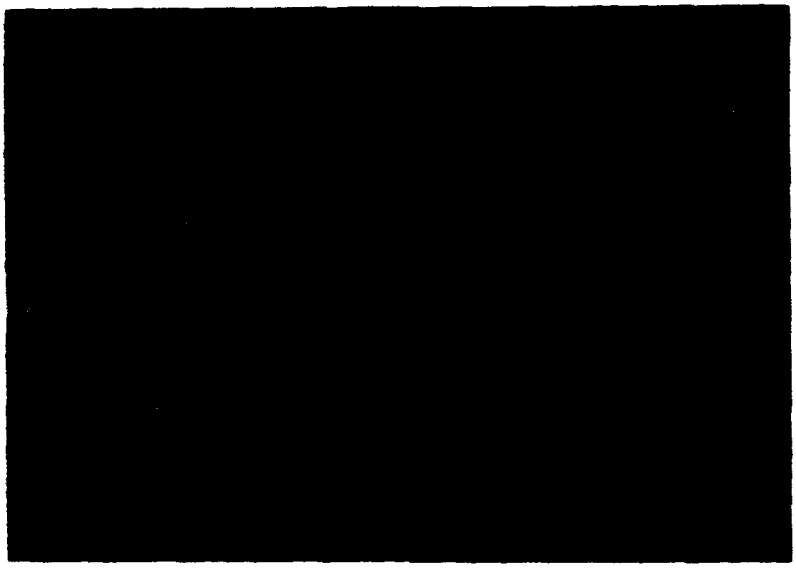

(e)

Figure 4.6 e) 100 hours.

SEM examination. Micrographs of these samples are shown in Figures 4.7 and 4.8. All micrographs show what appear to be recrystallized grain structures. The micrographs in Figure 4.7 show a large number of uniformly distributed, equiaxed, θ-phase precipitates. The grain contrast suggests a high degree of misorientation associated with the grain boundaries. Grains are not uniform in size, how ver, and range from very small to very large. Grain boundaries are mostly curved, which suggests grain boundary migration was occurring. Figure 4.8 shows samples overaged at higher temperatures with fewer total θ precipitates evident than Figure 4.7 since the overaging temperature is closer to the solvus and a smaller volume fraction of θ-phase particles will form. In addition, the θ precipitates in Figure 4.8 appear to have a broader size distribution than those in Figure 4.7. The degree of orientation contrast has decreased which suggests less difference in grain orientation. The grain size distribution is narrower than observed in Figure 4.7 and the grains have fewer curved facets which is more suggestive of polygonization rather than recrystallization for these higher overaging temperatures [Ref. 15]. The micrographs again illustrate the almost inconsequential effect of the initial 200°C overaging on the final microstructure.

A quantitative assessment of the average grain size of these recrystallized samples was made using the mean linear intercept method [Ref. 27]. Table 4.1 shows the results of these

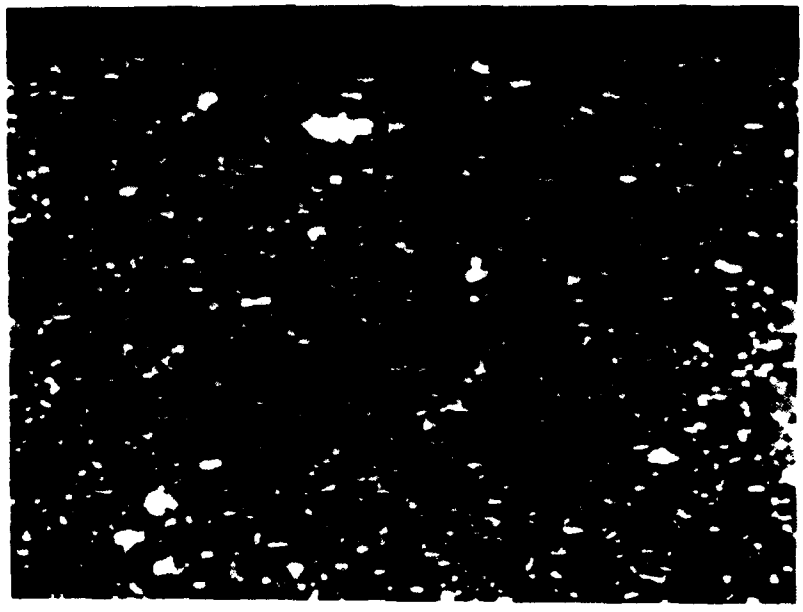

(a)

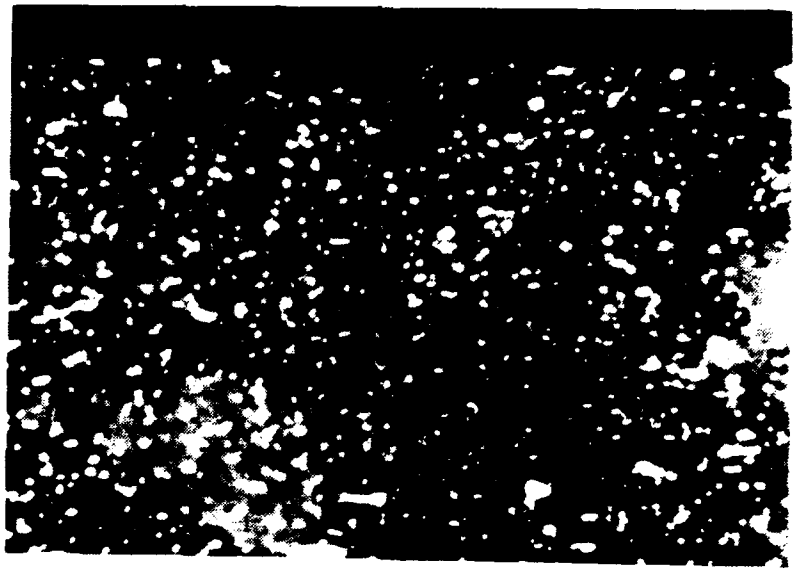

(b)

Figure 4.7 Backscattered electron micrographs showing grain orientation contrast of samples prestrained at 25°C and a secondary overaging of 50 hours at 400°C. Initial aging was conducted at 200°C for a) 50 hours; and b) 100 hours.

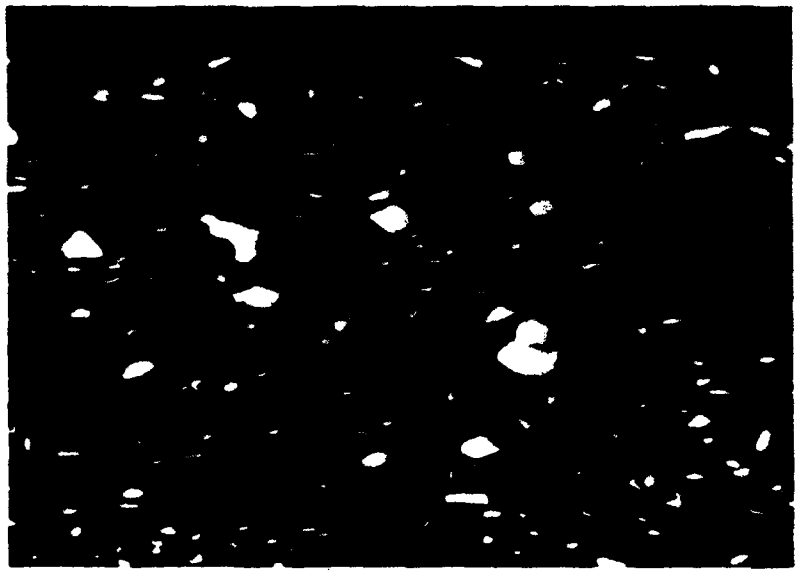

(a)

(b)

Figure 4.8 Backscattered electron micrographs showing grain orientation contrast of samples prestrained at 25°C and a secondary overaging for 50 hours at 450°C. Initial aging was conducted at 200°C for a) 50 hours; b) 100 hours.

measurements. The average grain size of 9.6μm is somewhat coarser than that reported in Rogers' work with a superplastic Al-Mg alloy [Ref. 25].

TABLE 4.1: AVERAGE GRAIN SIZE OF RECRYSTALLIZED SAMPLES

Overaging treatment	Average grain size (μm)
50 hours@200°C + 50 hours@400°C	9.6
50 hours@200°C + 50 hours@425°C	13.2
50 hours@200°C + 50 hours@450°C	12.5
100 hours@200°C + 50 hours@400°C	10.2
100 hours@200°C + 50 hours@425°C	12.0
100 hours@200°C + 50 hours@450°C	11.9
100 hours@200°C + 100 hours@400°C	11.1

Also, the grain size data is similar to that reported by Dunlap [Ref. 6].

B. IMAGE ANALYSIS

As previously discussed, histograms were developed from the data obtained using the Image-Pro software. These histograms supply the quantitative results from the micrographs. Although histograms were obtained to show major axis length, average diameter and aspect ratio of the θ-phase precipitates, it was

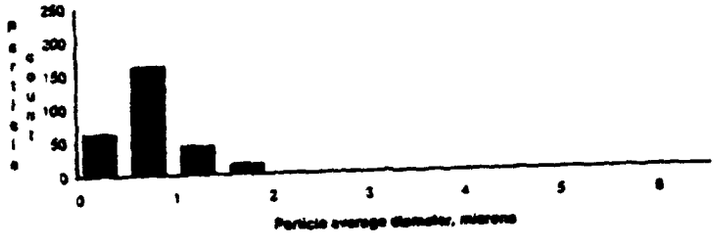

(a)

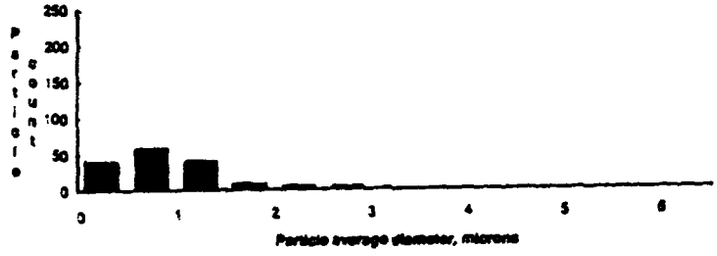

(b)

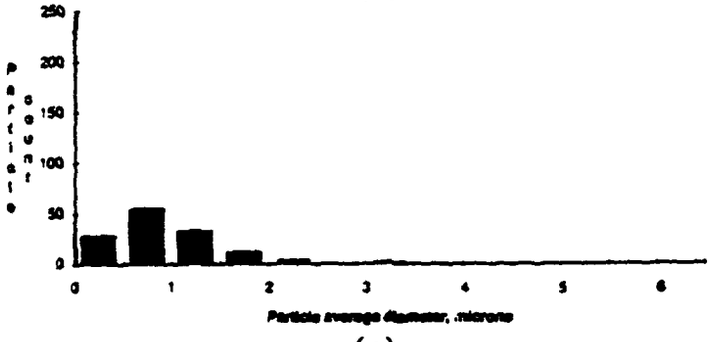

(c)

Figure 4.9 Histograms comparing the effect of increasing temperature at constant time on the particle's average diameter. All samples underwent a prestrain of 25°C and an initial aging of 200°C for 50 hours. Secondary overaging was conducted for 50 hours at a) 400°C; b) 425°C; c) 450°C.

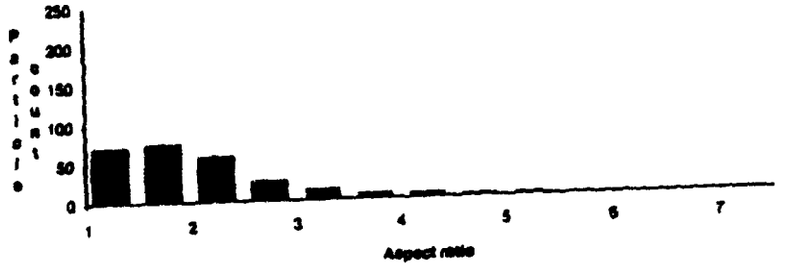

(a)

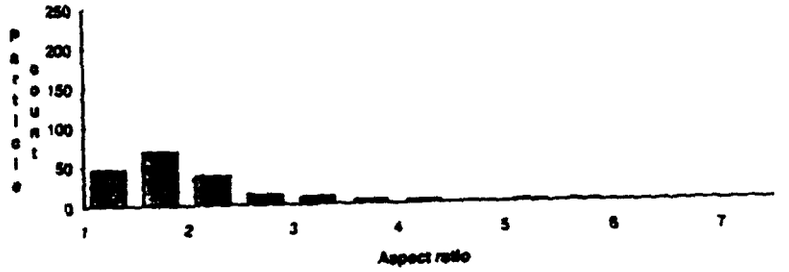

(b)

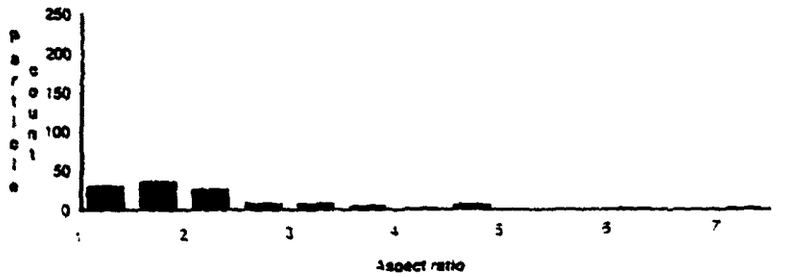

(c)

Figure 4.10 Histograms comparing the effect of constant time with increasing temperature on the particle's aspect ratio. All samples underwent a prestrain at 200°C and an initial aging of 200°C for 50 hours. Secondary overaging was conducted for 50 hours at a) 400°C; b) 425°C; c) 450°C.

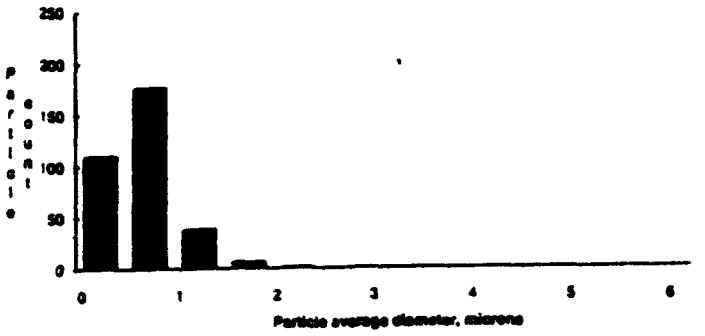

(a)

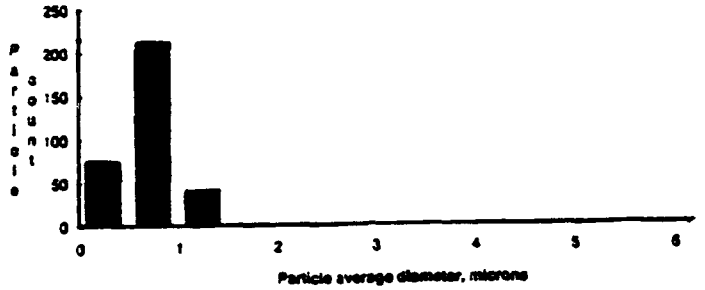

(b)

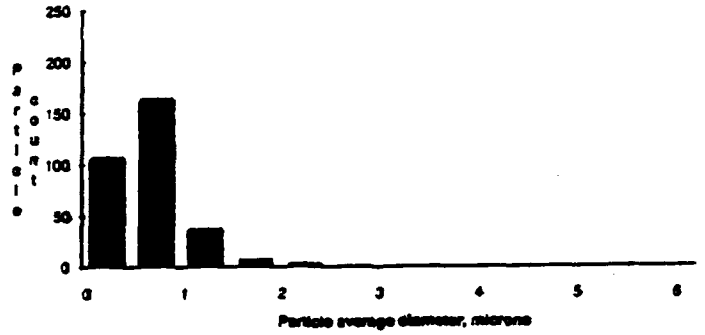

(c)

Figure 4.11 Histograms comparing the effect of initial overage time on the particle's average diameter. All samples underwent a prestrain of 25°C and a secondary aging of 400°C for 50 hours. Initial overaging was conducted at 200°C for a) 0 hours; b) 50 hours; and c) 100 hours.

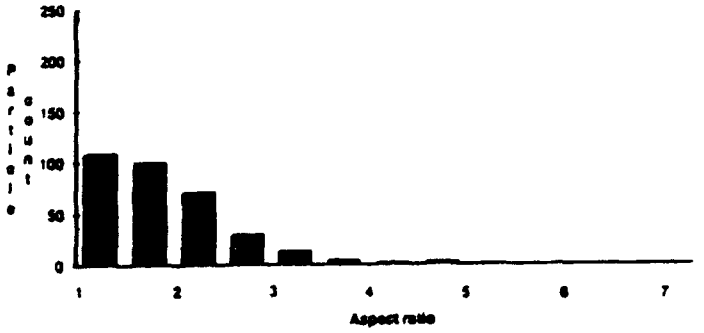

(a)

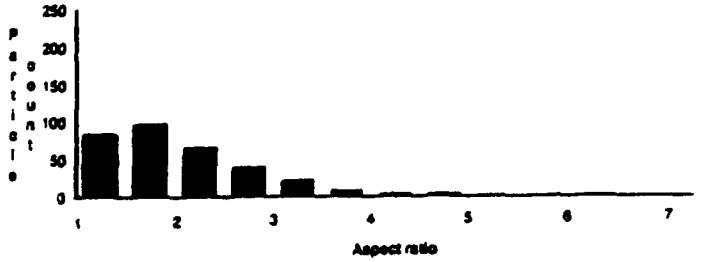

(b)

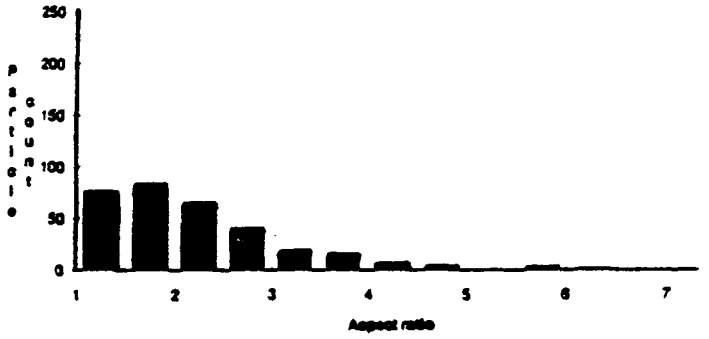

(c)

Figure 4.12 Histograms comparing the effect of initial overage time on the particle's aspect ratio. All samples underwent a prestrain of 25°C and a secondary aging of 400°C for 50 hours. Initial overaging was conducted at 200°C for a) 0 hours; b) 50 hours; and c) 100 hours.

apparent that the key parameters to examine were average diameter and aspect ratio.

For easier analysis, histograms are arranged with the same aging condition with respect to time and varying the temperature. These histograms show more narrow distribution of particles that are smaller in both size and aspect ratio for lower temperatures, and a broader distribution of sizes and aspect ratios at higher overaging temperatures. It was observed that the total number of particles counted decreased and the temperature increased, reflecting the approach to the solvus temperature.

Figures 4.9 and 4.10 were obtained from micrographs which include grain boundary particles. Image analysis was also conducted on micrographs which were taken of the center of the grain (matrix). Figure 4.9a is the histogram generated from image analysis of the micrograph shown in Figure 4.3a. Figure 4.11 shows histograms of the average diameter for samples that differed in the amount of initial overaging at 200°C. All show relatively narrow size distribution with no particles having a greater average diameter than 3μm. Aspect ratio histograms, presented in Figure 4.12, suggest a similar pattern except that the distribution becomes broader as the initial overaging time increases. These results confirm the earlier observation that the initial overaging at 200°C does not affect the overall microstructure to a great extent. Histograms in Figures 4.11 and 4.12 were made after image analysis of the micrographs shown in Figure 4.5. Table 4.2 summarizes the

mean average diameters of the samples shown in Figure 4.11. Average diameter, using the Image-Pro software, is the length of five chords (rotated incrementally) which measure the size of a particle through its centroid divided by five. The mean average diameter is the value which represents the total of all particle average diameters in a given field of view divided by the total number of particles.

TABLE 4.2: MEAN AVERAGE PARTICLE DIAMETER OF SELECTED SAMPLES FROM IMAGE ANALYSIS

Overaging treatment	Mean average diameter (μm)
0 hours@200°C + 50 hours@400°C	0.7
50 hours@200°C + 50hours@400°C	0.7
100 hours@200°C + 50 hours@400°C	0.7

One further comparison, shown in Figures 4.13 and 4.14, is made between samples which underwent the same overaging schedule but differed in their prestrain temperature. Average diameter histograms between the two prestrain temperatures in Figure 4.13 show a greater number of total particles were counted for the 25°C prestrain and the size distribution is slightly more narrow. The histograms illustrating aspect ratio differences in Figure 4.14 again show a wider distribution for the 200°C prestrain.

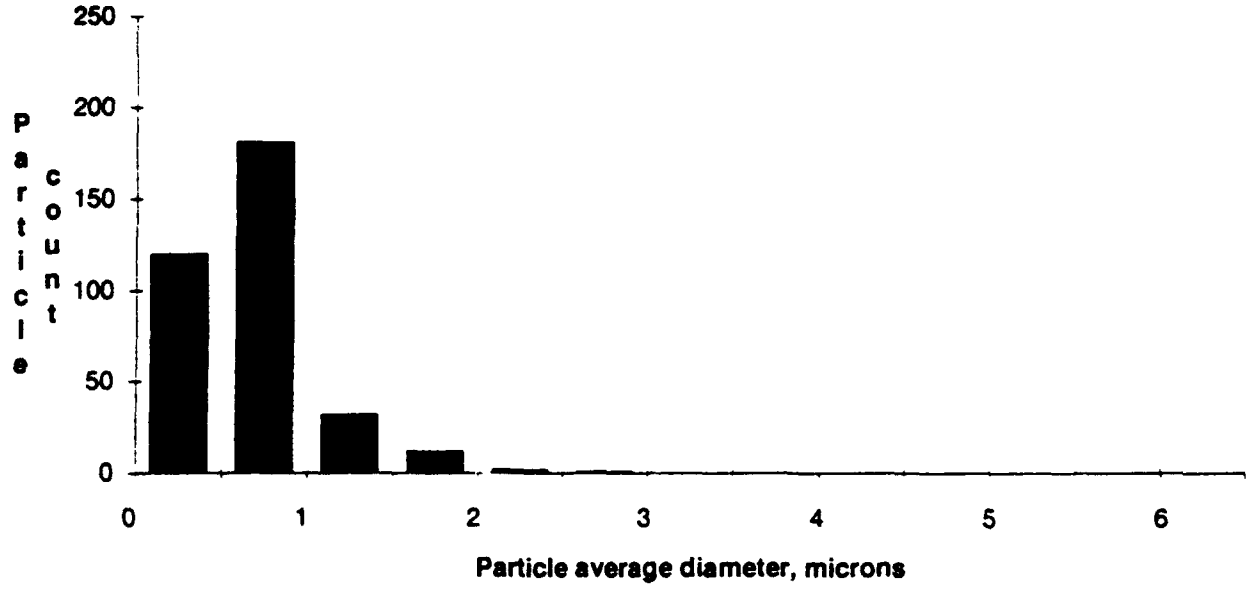

(a)

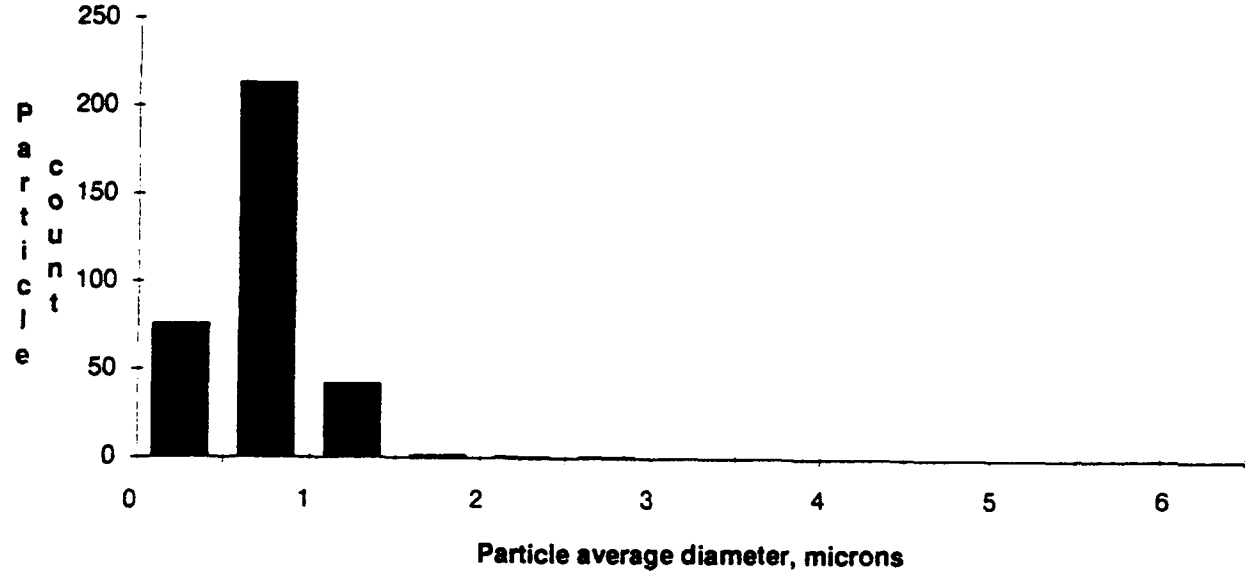

(b)

Figure 4.13 Histograms comparing the effect of prestrain temperature on the particle's average diameter. Both samples underwent an aging sequence of 200°C for 50 hours and 400°C for 50 hours. The prestrain temperature was a) 200°C ; and b) 25°C.

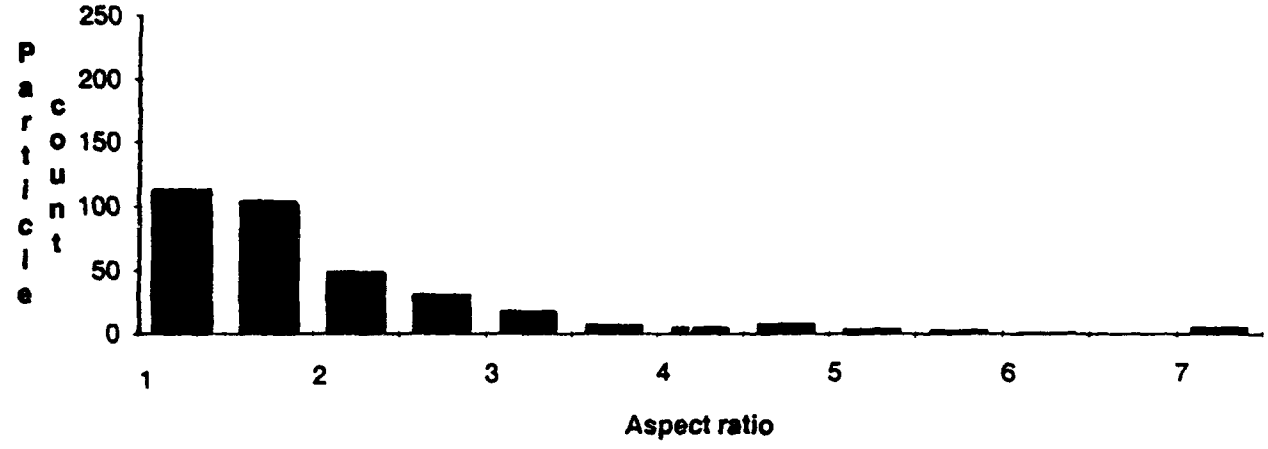

(a)

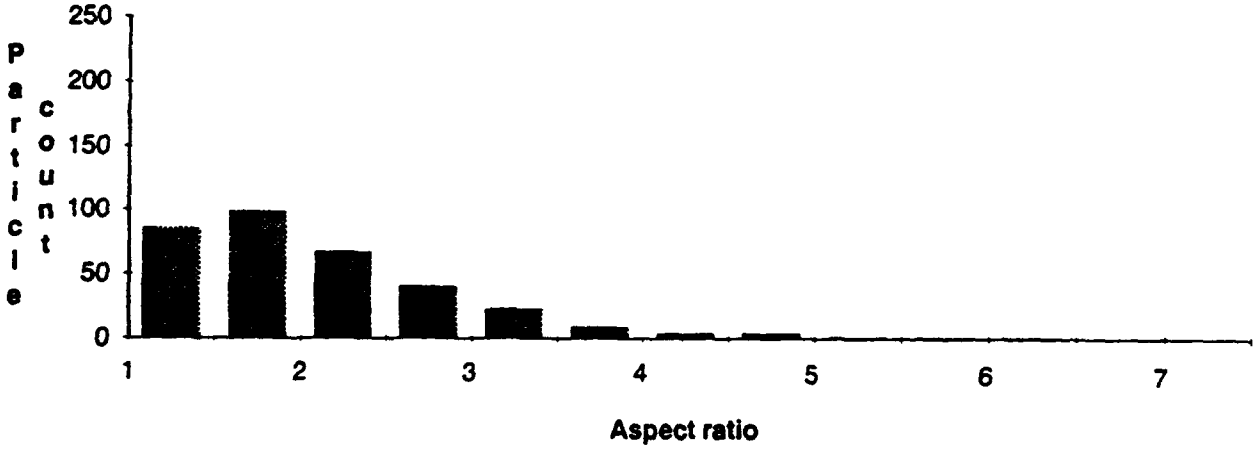

(b)

Figure 4.14 Histograms comparing the effect of prestrain temperature on the particle's aspect ratio. Both samples underwent an aging sequence of 200°C for 50 hours and 400°C for 50 hours. The prestrain temperature was a) 200°C ; and b) 25°C.

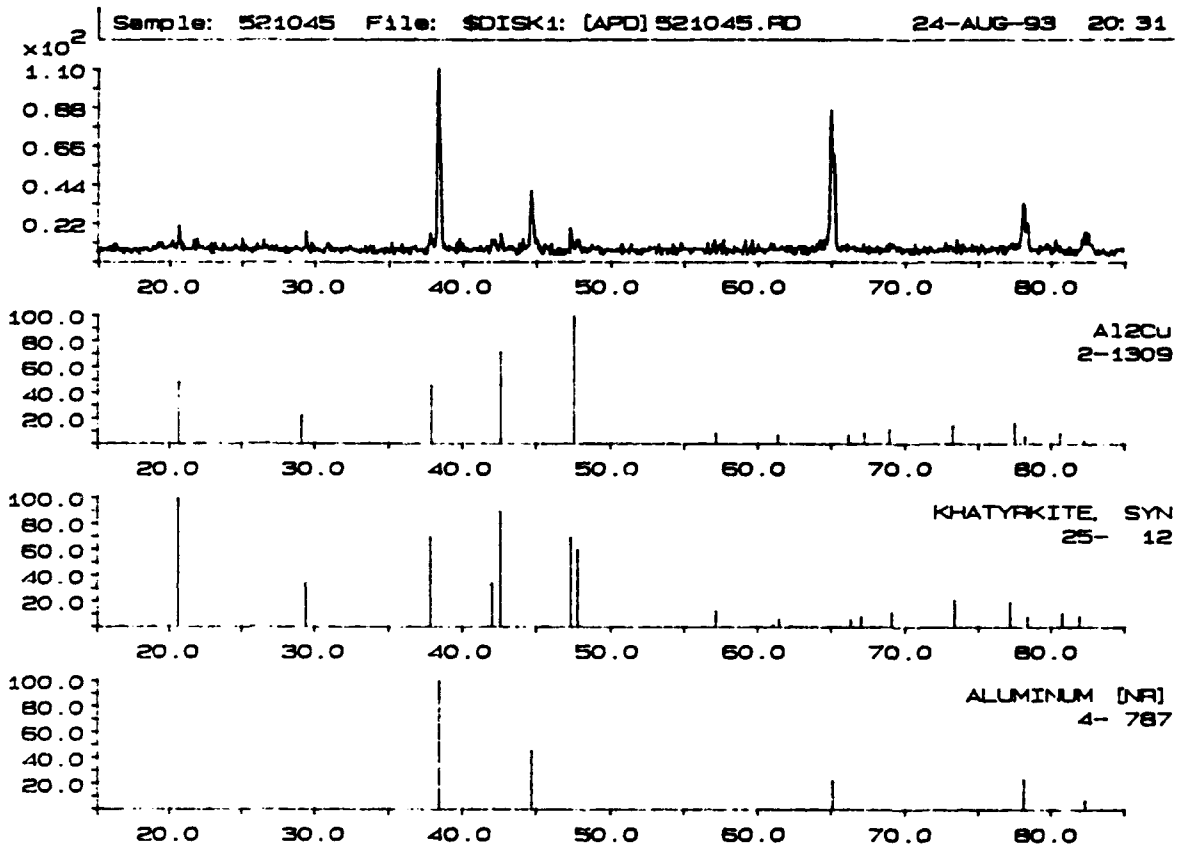

Figure 4.15 X-ray diffraction results confirming the presence of Aluminum, Al_2Cu and Khatyrkite ($CuAl_2$).

These data indicate that overaging at a higher temperature in the range 400-450°C does not produce appreciably coarser particles. Instead, fewer particles are seen as the temperature approaches the solvus temperature for the alloy. Dunlap's analysis [Ref. 6] suggested d_{crit} is 2.0μm or more and thus more prolonged aging at a lower temperature would appear to be necessary to produce a large number of critical-size particles.

C. X-RAY DIFFRACTION

X-ray diffraction results shown in Figure 4.15 confirm the presence of Aluminum, Al_2Cu and Khatyrkite ($CuAl_2$). Khatyrkite data will supersede Al_2Cu data since it has recently found to be more complete. This shows the presence of θ precipitates.

D. ROLLING

General observations of the rolling process indicate a longer IPA time or a higher IPA temperature is required. Samples rolled at a five minute IPA demonstrated severe "alligatoring" and samples with a 30 minute IPA showed only edge cracking. Despite these problems all samples were able to complete the nine pass rolling schedule. Alligatoring results when rolling causes the sample surfaces to be placed in tension and the center to be placed in compression. Fracture results when a metallurgical weakness is encountered on the centerline in combination with the above conditions. Edge cracking results from unequal transverse frictional forces. This causes the center to decrease in thickness and the sample length to increase while only part of the edge thickness

decrease goes to the sample length increase. This causes strains in the sheet and leads to edge cracking [Ref. 28]. Although some of the blame for these cracking problems is based upon the mill geometry, changes in the IPA appear to be beneficial.

V. CONCLUSIONS AND RECOMMENDATIONS

A. CONCLUSIONS

Considering the various processes utilized in this research and the different TMPs employed as well as a quantitative and qualitative analysis of the data, the following conclusions were reached:

1. Prestrain performed at 25°C resulted in a more uniform particle distribution and produced finer and fewer θ precipitates at the grain boundaries than the prestrain performed at 200°C. Also, prestrain conducted at 25°C show smaller PFZ than the 200°C prestrain.
2. The initial aging (pre-aging) time at 200°C has no effect on the number or size of the θ precipitates developed during subsequent aging at 400°C.
3. The sample that was prestrained at 25° C and aged for 50 hours at 200°C and 50 hours at 400°C shows the greatest promise for achieving sufficient grain refinement for superplasticity in this work.
4. Overaging conducted at 350°C resulted in θ precipitates that were too small and overaging at 450°C shows θ precipitates to be too few in number.

B. RECOMMENDATIONS

For further research in this field, the following recommendations are made:

1. Eliminate initial low temperature overaging and concentrate further overaging between the temperatures of 375°C and 425°C.
2. Utilize the image analysis software to determine the particles nearest neighbor distances to better assess particle distribution.
3. Modify IPA time and/or temperature as necessary to avoid cracking during rolling.
4. Perform further annealing experiments over a range of temperatures and times for optimal grain refinement.
5. Perform transmission electron microscopy to confirm particle composition and assess grain/subgrain boundaries.
6. Perform tensile tests at elevated temperatures to determine if the alloy demonstrates superplastic elongation.
7. Perform x-ray texture analysis to determine grain orientation.

LIST OF REFERENCES

1. Tang, S., *Mechanics of Superplasticity*, Robert E. Krieger Publishing Co., Inc., 1979.

2. Northrop Corporation, Aircraft Division, *Superplastic Forming: Precision Technology for Building New Generations of Aircraft*, Hawthorne, CA, 1983.

3. Mathe, W., *Precipitate Coarsening During Overaging of 2519 Al-Cu Alloy: Application to Superplastic Response*, Master's Thesis, Naval Postgraduate School, Monterey, CA, March 1992.

4. Bohman, S., *Thermomechanical Processing of Aluminum Alloy for Grain Refinement and Superplasticity*, Master's Thesis, Naval Postgraduate School, Monterey, CA, June 1992.

5. Humphreys, F. J., "Local Lattice Rotations at Second Phase Particles in Deformed Metals," *Scripta Metallurgica*, Vol. 27, pp. 1801-1814, 1979.

6. Dunlap, J., *Study of Refinement in Al Alloy 2519 Using Backscatter Orientation - Contrast Made in the Scanning Electron Microscope*, Master's Thesis, Naval Postgraduate School, Monterey, CA, December 1992.

7. McNelley, T. R. and Hales, S. J., "The Roles of Zr and Mn in Processing and Superplasticity of Al-Mg Alloys," *Superplasticity in Aerospace II*, ed. T. R. McNelley and H. C. Heikkenen, The Minerals, Metals and Materials Society, pp. 207-222, 1990.

8. Callister, W. D., *Materials Science and Engineering: An Introduction*, 2nd edition, John Wiley and Sons, Inc., New York, NY, 1984.

9. Staley, J. T., "History of Wrought Aluminum Alloy Development, *Aluminum Alloys - Contemporary Research and Applications*, ed. A. K. Vasudevan and R. D. Doherty, Academic Press, Inc., San Diego, CA, 1989.

10. "Binary Alloy Phase Diagrams, *American Society for Metals*, Vol. 1, Metals Park, OH, 1986.

11. Lorimer, G. W., "Precipitation in Aluminum Alloys," *Precipitation Processes in Solids*, ed. K. C. Russell and H. I. Aaronson, American Institute of Mining, Metallurgical and Petroleum Engineers, New York, NY, 1978.

12. Porter, D. A., and Easterling, K. E., *Phase Transformations in Metals and Alloys*, Van Nostrand Reinhold Co., Ltd., Wokingham, England, 1988.

13. Martin, J. W., *Precipitation Hardening*, Pergamon Press, Ltd., Oxford, 1968.

14. Smallman, R.E., *Modern Physical Metallurgy*, Butterworths, 1990.

15. Shewmon, P. G., *Transformations in Metals*, McGraw-Hill Book Company, p. 88, 1969.

16. Wert, J. A., "Grain Refinement and Grain Size Control," *Superplastic Forming of Structural Alloys*, ed. N. E. Paton and C. Hamilton, Conference Proceedings, TMS-AIME, Warrendale, PA, 1982.

17. Watts, B. M., Stowell, M. J., Baikie, B. L. and Owen, D. G. E., "Superplasticity in Al-Cu-Zr Alloys, Parts I & II," *Metal Science Journal*, Vol. 10, No. 6, pp. 189-206, 1976.

18. Hamilton, C. H., Bampton, C. C., and Paton, N. E., "Superplasticity in High Strength Aluminum Alloys," *Superplastic Forming of Structural Alloys*, ed. N. E. Paton and C. H. Hamilton, Conference proceedings, TMS-AIME, Warrendale, PA, pp. 173-189, 1982.

19. Ashby, M. F., *Philos. Metall.*, 21 (1970) 399.

20. Argon, A. S., Im, J. and Safoglu, R., "Cavity Formation From Inclusions in Ductile Fracture," *Metallurgical Transactions*, Vol. 6A, p. 82, 1975.

21. Humphreys, F. J., Acta. Metall., 25 (1977) 1323.

22. McNelley, T. R., Crooks, R., Kalu, P. N., Rogers, S. A., "Precipitation and Recrystallization During Processing of a Superplastic Al-10Mg-0.1 Zr Alloy," *Material Science and Engineering*, A166, pp. 135-143, 1993.

23. Willig, V., and Heimendahl, M., *"Problems of Particle Coarsening of Disk Shaped Particles in Aluminum Alloy 2219,"* Institut fur Wefkstoffwissenschaften 1 der Universitas Erlangen, Nurnberg, 674-681, 1979.

24. Hales, S. J., McNelley, T. R., and McQueen, H.J., "Recrystallization and Superplasticity at 300°C in an Aluminum-Magnesium Alloy," *Metallurgical Transactions*, Vol. 22A, pp. 1037-1047, 1991.

25. Rogers, S., *The Role of Particles in Recrystallization of a Thermomechanically Processed Al-Mg Alloy*, Master's Thesis, Naval Postgraduate School, Monterey, CA, 1992.

26. Martin, J. W., and Doherty, *Stability of Microstructure in Metallic Systems*, Cambridge University Press, Cambridge, 1976.

27. *Metals Handbook*, 8th ed., vol. 8, American Society for Metals, p. 47, 1973.

28. Dieter, G. E., *Mechanical Metallurgy*, 2nd ed., McGraw-Hill International, pp. 601-607, 1981.

INITIAL DISTRIBUTION LIST

1.	Defense Technical Information Center Cameron Station Alexandria, VA 22304-6145	2
2.	Library, Code 52 Naval Postgraduate School Monterey, CA 93943-5002	2
3.	Naval Engineering, Code 34 Naval Postgraduate School Monterey, CA 93943-5100	1
4.	Department Chairman, Code ME/Kk Department of Mechanical Engineering Naval Postgraduate School Monterey, CA 93943-5000	1
5.	Professor T.R. McNelley, Code ME/Mc Department of Mechanical Engineering Naval Postgraduate School Monterey, CA 93943-5000	4
6.	Adjunct Professor R. Crooks, Code ME/Cc Department of Mechanical Engineering Naval Postgraduate School Monterey, CA 93943-5000	1
7.	Peter J. Zohorsky 2316 Seabury Drive Crofton, MD 21114	2